Modeling and Analysis of Dual Three-Phase Self-Excited Induction Generator for Wind Energy Conversion Systems

Magno Ayala[1], Osvaldo Gonzalez[1], Jorge Rodas[1], Raul Gregor[1], Jesus Doval-Gandoy[2] and Marco Rivera[3]

[1]*Laboratory of Power and Control Systems, Facultad de Ingeniería, Universidad Nacional de Asunción, Paraguay*

E-mail: {mayala, ogonzalez, jrodas & rgregor}@ing.una.py

[2]*Applied Power Electronics Technology Research Group, Universidad de Vigo, Spain.* E-mail: jdoval@uvigo.es

[3]*Department of Electrical Engineering, Universidad de Talca, Chile.* E-mail: marcoriv@utalca.cl

***Abstract*—Multiphase self-excited induction generators have recently become more interesting due to its advantages compared to its equivalent three-phase generator such as post-fault operations and lower torque ripple. However, as an induction generator, it has some disadvantages regarding poor voltage and frequency regulation under varying load and speed regimes. A steady state analysis is fundamental to comprehend the machine's behavior. For a more precise modeling, it is considered a non-linear variation of the magnetizing inductance. This paper presents a detailed mathematical model and analysis of the dual three-phase self-excited induction generator for wind energy conversion systems connected to different loads. Simulation results are provided to show the behavior of the machine and its build up voltage through different conditions.**

***Index Terms*—Magnetizing inductance, minimum capacitance, multiphase machines, renewable energy, self-excited induction generator.**

NOMENCLATURE

DTP	Dual three-phase.
SEIG	Self-excited induction generators.
VSC	Voltage source converters.
WECS	Wind energy conversion systems.

I. INTRODUCTION

Renewable energy systems using small-hydro and wind power are active areas of research. Three-phase induction generators are mainly employed in such systems because of their reliability, low cost, simple construction, ruggedness and low maintenance [1]. However, it is inconvenient to apply for high power generation as it fails to operate with fault on one or more phases on stator. It also produces a notorious torque ripple with high amplitude and low frequency and a high mechanical vibration [1], [2]. Thus, the interest in multiphase machines has risen due to intrinsic features such as lower torque ripple, power splitting or better fault tolerance than three-phase machines. Current research works and developments support the prospect of future more widespread applications of multiphase machines [2]. In industrial applications, any multiphase machine would be operated under variable-speed conditions, meaning that a multiphase power electronic converter is required [3]. At the same time, multiphase generation systems appear in renewable applications in recent times, particularly in stand-alone and grid-connected WECS [4]. Among the most common generations systems, WECS are increasingly becoming more cost competitive comparing to all the environmentally safe and clean renewable energy sources. Fixed speed WECS have gained much popularity among the manufacturers and developers in this field mainly due to the fact that fixed speed wind turbines uses a squirrel cage induction generator [5]. The design of larger wind turbines and reliability requirements match the features of multiphase machines due to their capability to split power and provide fault tolerance. The most investigated option has been the use of DTP SEIG connected by two-level VSCs [6]. SEIGs are a good option for WECS especially in remote areas, because they do not need any external source of power supply to produce the required excitation magnetic field. Permanent magnet generators may also be used for wind energy applications, however, the generated voltage increases linearly with the wind turbine speed. SEIG can cope with a small increase in speed from their rated value because, due to saturation, the increasing rate of the generated voltage is not linear with the mechanical speed [7]. Understanding the voltage terminal build up process of SEIG and its performance under steady state and dynamic condition, it becomes a fundamental step toward the development of more efficient and competitive SEIG technology [5], [7]. For a SEIG, the external elements that can modify the voltage profile are the mechanical speed, the terminal capacitance and the connected load impedance [8], [9]. In this work, the SEIG is analyzed with several types of loads (no load, a resistive load and a RL load).

This paper presents a mathematical model and analysis of a DTP SEIG for WECS. The voltage build up process and the behavior through different loads is analyzed by using the MATLAB/Simulink program. The modeling is tested under different conditions.

This work is organized as follows: Section II analyzes the mathematical model of the DTP SEIG. Section III details the magnetizing inductance behavior and the self-excitation process. Simulation results are provided in Section IV, showing the output voltage under different conditions. The conclusions are finally summarized in the last section.

II. Self Excited Induction Generator Model

The mathematical model of the DTP SEIG is very similar to the DTP induction motor. However, the DTP SEIG has a capacitor bank connected to its terminals, which has to be considered in this model. Besides, in this case, the rotor speed, provided by the turbine, is considered as an input, unlike the motor case [10], [11].

In order to analyze the mathematical model of the DTP SEIG, first it is necessary to convert the six-phase (a-b-c-d-e-f) to a (α-β)-(x-y)-(z_1-z_2) model using Clark's transformation proposed in [12].

In this section, it is presented the mathematical model in the (α-β)-(x-y) stationary frame to study both transient and steady state behaviors during the voltage build up process, the modeling of excitation system with a RL load. The equivalent electric circuit of a DTP SEIG is shown in Fig 1.

From Fig 1, we have $C_{\alpha s}$, $C_{\beta s}$ and C_{xys}, $C_{z_1 z_2 s}$ which are capacitances from the (α-β), (x-y) and (z_1-z_2) sub-space respectively. R_s and R_r are resistances from the stator and rotor. L_{ls} and L_{lr} are dispersion inductances from the stator and rotor. L_m is the magnetizing inductance, ω_r is the electrical speed of the motor. $\lambda_{\alpha r}$ and $\lambda_{\beta r}$ are rotor flux linkages from (α-β) sub-space. $I_{\alpha s}$ and $I_{\alpha r}$ are stator and rotor currents from α sub-space. $I_{\beta s}$ and $I_{\beta r}$ are stator and rotor currents from β sub-space. $I_{m\alpha}$ and $I_{m\beta}$ are magnetizing currents from (α-β) sub-space. I_{xys} and $I_{z_1 z_2 s}$ are stator currents from (x-y) and (z_1-z_2) sub-spaces.

For two isolated neutrals configuration, both (z_1-z_2) currents cannot flow, so the components of the (z_1-z_2) sub-space can be ignored [13].

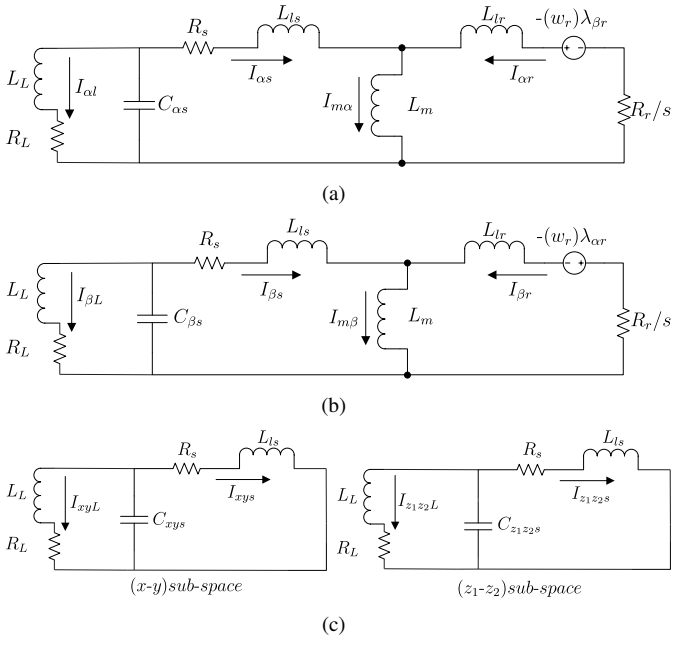

Fig. 1. Equivalent circuit of the DTP SEIG in: (a) α sub-space; (b) β sub-space; (c) (x-y) and (z_1-z_2) sub-space.

The equations, which describe the circuits representing the DTP SEIG, are based on the equilibrium equation of voltage:

$$\begin{aligned} V_{c\alpha s} + R_s I_{\alpha s} + \frac{d}{dt}\lambda_{\alpha s} &= 0 \\ R_r I_{\alpha r} - \omega_r \lambda_{\beta r} + \frac{d}{dt}\lambda_{\alpha r} &= 0 \\ V_{c\beta s} + R_s I_{\beta s} + \frac{d}{dt}\lambda_{\beta s} &= 0 \\ R_r I_{\beta r} + \omega_r \lambda_{\alpha r} + \frac{d}{dt}\lambda_{\beta r} &= 0 \end{aligned} \tag{1}$$

where $\frac{d}{dt}$ is the differential operator and $V_{c\alpha s}$ and $V_{c\beta s}$ are the capacitor voltages, which are:

$$\begin{aligned} V_{c\alpha s} &= \tfrac{1}{C_{\alpha s}} \int I_{\alpha s}\, dt + V_{c\alpha s0} \\ V_{c\beta s} &= \tfrac{1}{C_{\beta s}} \int I_{\beta s}\, dt + V_{c\beta s0} \end{aligned} \tag{2}$$

where $V_{c\alpha s0} = V_{c\alpha s}|_{t=0}$ and $V_{c\beta s0} = V_{c\beta s}|_{t=0}$ are the initial capacitor voltages. Stator windings flow links are related to the stator and rotor currents by:

$$\begin{aligned} \lambda_{\alpha s} &= L_s I_{\alpha s} + L_m I_{\alpha r} \\ \lambda_{\beta s} &= L_s I_{\beta s} + L_m I_{\beta r} \end{aligned} \tag{3}$$

and the rotor windings flow links are given by:

$$\begin{aligned} \lambda_{\alpha r} &= L_r I_{\alpha r} + L_m I_{\alpha s} + \lambda_{\alpha r0} \\ \lambda_{\beta r} &= L_r I_{\beta r} + L_m I_{\beta s} + \lambda_{\beta r0} \end{aligned} \tag{4}$$

where $\lambda_{\alpha r0}$ and $\lambda_{\beta r0}$ are the links residual flow in (α-β) sub-space. L_s and L_r are the inductances of the stator and rotor windings, respectively, and are given by:

$$\begin{aligned} L_s &= L_{ls} + L_m \\ L_r &= L_{lr} + L_m \end{aligned} \tag{5}$$

ω_r, $\lambda_{\alpha r}$ and $\lambda_{\beta r}$ produce a rotational voltage, so, this is equivalent to these equations:

$$\begin{aligned} \omega_r \lambda_{\alpha r} &= \omega_r (L_r I_{\alpha r} + L_m I_{\alpha s} + \lambda_{\alpha r0}) \\ \omega_r \lambda_{\alpha r} &= \omega_r (L_r I_{\alpha r} + L_m I_{\alpha s}) + K_{\beta r} \\ \omega_r \lambda_{\beta r} &= \omega_r (L_r I_{\beta r} + L_m I_{\beta s} + \lambda_{\beta r0}) \\ \omega_r \lambda_{\beta r} &= \omega_r (L_r I_{\beta r} + L_m I_{\beta s}) + K_{\alpha r} \end{aligned} \tag{6}$$

where $K_{\alpha r} = \omega_r \lambda_{\alpha r0}$ and $K_{\beta r} = \omega_r \lambda_{\beta r0}$ are induced initial voltages caused by the residual magnetic flux in the (α-β) sub-space.

By replacing (3) and (6) in (1), it is obtained the group of equations which describe the DTP SEIG in the stationary reference frame. Thus we have:

$$
\begin{aligned}
&V_{c\alpha s} + R_s I_{\alpha s} + L_s \frac{d}{dt} I_{\alpha s} + L_m \frac{d}{dt} I_{\alpha r} = 0 \\
&V_{c\beta s} + R_s I_{\beta s} + L_s \frac{d}{dt} I_{\beta s} + L_m \frac{d}{dt} I_{\beta r} = 0 \\
&- K_{\alpha r} - \omega_r L_m I_{\beta s} + R_r I_{\alpha r} - \omega_r L_r I_{\beta r} \\
&+ L_m \frac{d}{dt} I_{\alpha s} + L_r \frac{d}{dt} I_{\alpha r} = 0 \\
&K_{\beta r} + \omega_r L_m I_{\alpha s} + R_r I_{\beta r} + \omega_r L_r I_{\alpha r} \\
&+ L_m \frac{d}{dt} I_{\beta s} + L_r \frac{d}{dt} I_{\beta r} = 0
\end{aligned} \tag{7}
$$

Eq. (7) can be written with a matrix form:

$$
\begin{bmatrix} 0 \\ 0 \\ 0 \\ 0 \end{bmatrix} = \begin{bmatrix} R_s & 0 & 0 & 0 \\ 0 & R_s & 0 & 0 \\ 0 & -\omega_r L_m & R_r & -\omega_r L_r \\ \omega_r L_m & 0 & \omega_r L_r & R_r \end{bmatrix} \begin{bmatrix} I_{\alpha s} \\ I_{\beta s} \\ I_{\alpha r} \\ I_{\beta r} \end{bmatrix} + \begin{bmatrix} L_s & 0 & L_m & 0 \\ 0 & L_s & 0 & L_m \\ L_m & 0 & L_r & 0 \\ 0 & L_m & 0 & L_r \end{bmatrix} \begin{bmatrix} \dot{I}_{\alpha s} \\ \dot{I}_{\beta s} \\ \dot{I}_{\alpha r} \\ \dot{I}_{\beta r} \end{bmatrix} + \begin{bmatrix} V_{c\alpha s} \\ V_{c\beta s} \\ -K_{\alpha r} \\ K_{\beta r} \end{bmatrix} \tag{8}
$$

From (8), clearing the derivatives of currents we obtain the simulation model for the DTP SEIG. In this way we get:

$$
\begin{bmatrix} \dot{I}_{\alpha s} \\ \dot{I}_{\beta s} \\ \dot{I}_{\alpha r} \\ \dot{I}_{\beta r} \end{bmatrix} = \frac{1}{Laux} \left\{ \begin{bmatrix} L_s & 0 & -L_m & 0 \\ 0 & L_s & 0 & -L_m \\ -L_m & 0 & L_r & 0 \\ 0 & -L_m & 0 & L_r \end{bmatrix} \right.
$$

$$
\left. - \begin{bmatrix} R_s & 0 & 0 & 0 \\ 0 & R_s & 0 & 0 \\ 0 & -\omega_r L_m & R_r & -\omega_r L_r \\ \omega_r L_m & 0 & \omega_r L_r & R_r \end{bmatrix} \begin{bmatrix} I_{\alpha s} \\ I_{\beta s} \\ I_{\alpha r} \\ I_{\beta r} \end{bmatrix} + \begin{bmatrix} -V_{c\alpha s} \\ -V_{c\beta s} \\ K_{\alpha r} \\ -K_{\beta r} \end{bmatrix} \right\} \tag{9}
$$

where:

$$
Laux = L_s L_r - L_m^2 \tag{10}
$$

which is obtained by clearing from Eq. (8).

For a resistive-inductive load (RL) the components of differential load voltage equations can be written as:

$$
\begin{aligned}
\frac{dV_{\alpha L}}{dt} &= \frac{1}{C_{\alpha s}} I_{\alpha C_{\alpha s}} \\
\frac{dV_{\beta L}}{dt} &= \frac{1}{C_{\beta s}} I_{\beta C_{\beta s}}
\end{aligned} \tag{11}
$$

where $I_{\alpha C_{\alpha s}} = I_{\alpha s} - I_{\alpha L}$ and $I_{\beta C_{\beta s}} = I_{\beta s} - I_{\beta L}$.

The components of differential load current equations can be written as:

$$
\begin{aligned}
\frac{dI_{\alpha L}}{dt} &= \frac{1}{L_L}(V_{\alpha L} - R_{L I_{\alpha L}}) \\
\frac{dI_{\beta L}}{dt} &= \frac{1}{L_L}(V_{\beta L} - R_{L I_{\beta L}})
\end{aligned} \tag{12}
$$

The mechanical part of the electrical drive is given by the following equations:

$$
T_g = 3P\left(\lambda_{\alpha s} I_{\beta s} - \lambda_{\beta s} I_{\alpha s}\right) \tag{13}
$$

$$
J\frac{d}{dt}\omega_r + B\omega_r = P\left(T_i - T_g\right) \tag{14}
$$

where T_i denotes the input torque, T_g is the generated torque, J the inertia coefficient, P the number of pairs of poles and B the friction coefficient.

The equations in (x-y) sub-space do not link to the rotor side and consequently do not contribute to the air-gap flux, nonetheless, they are an important source of energy losses. These equations can be written as:

$$
\begin{bmatrix} V_{cxs} \\ V_{cys} \end{bmatrix} = \begin{bmatrix} L_{ls} & 0 \\ 0 & L_{ls} \end{bmatrix} \frac{d}{dt} \begin{bmatrix} I_{cxs} \\ I_{cys} \end{bmatrix} + \begin{bmatrix} R_s & 0 \\ 0 & R_s \end{bmatrix} \begin{bmatrix} I_{cxs} \\ I_{cys} \end{bmatrix} \tag{15}
$$

As mentioned before, (9)-(15) represent the simulation model for the DTP SEIG.

III. Magnetizing Inductance and Self-Excitation Process Analysis

The variation of the magnetizing inductance is the main factor in the dynamics of the voltage build up and stabilization in DTP SEIGs. The relationship between the magnetizing inductance L_m and magnetizing current I_m is obtained experimentally from open-circuit test at synchronous speed with the DTP SEIG parameters listed in Table I.

The magnetizing inductance curve as function of the magnetizing current is given in Fig. 2 and it is a nonlinear function, which can be represented by a four order polynominal curve fit, obtained through the MATLAB/Simulink software. The experimental setup details can be found in [10].

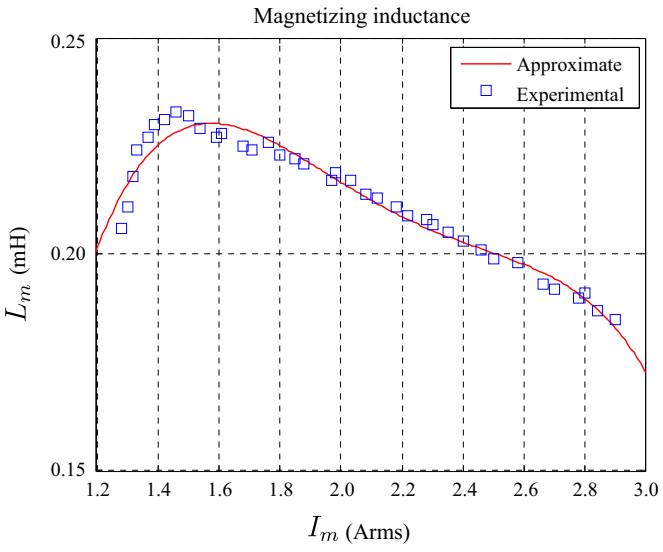

Fig. 2. Magnetizing inductance curve related to the magnetizing current.

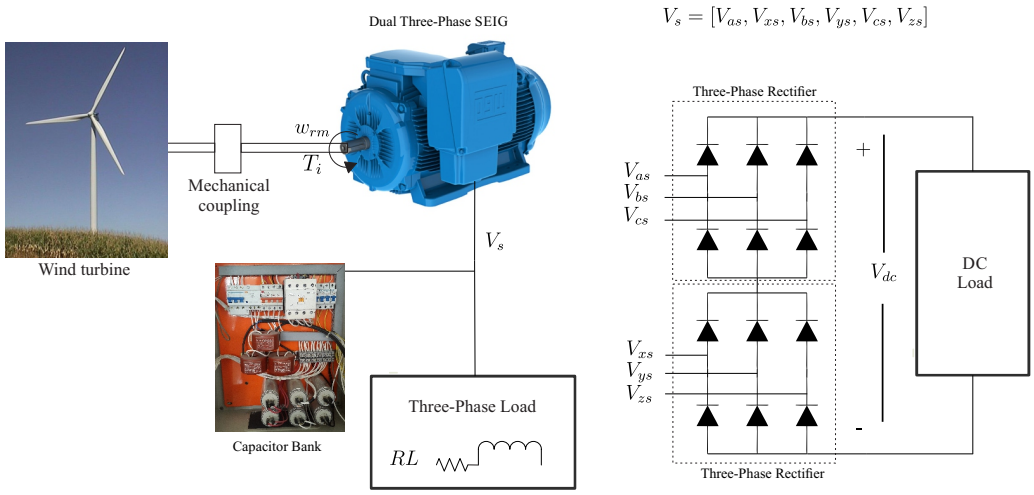

Fig. 3. Block diagram of a DTP SEIG for WECS.

$$L_m = -0.0667I_m^4 + 0.5901I_m^3 - 1.93I_m^2 + 2.7304I_m - 1.1774 \tag{16}$$

where the measured magnetizing current is:

$$I_m = \frac{\sqrt{I_{m\alpha}^2 + I_{m\beta}^2}}{\sqrt{2}} \tag{17}$$

where $I_{m\alpha} = I_{\alpha s} + I_{\alpha r}$ and $I_{m\beta} = I_{\beta s} + I_{\beta r}$

The DTP SEIG requires a minimal value for the mechanical rotor speed and the capacitance connected to the stator terminals of the DTP SEIG. An effective way to obtain it for the self-exciting process is through the next equation:

$$C_{min} = \frac{1}{P^2 \omega_{rm}^2 M} \approx 51\mu F \tag{18}$$

where ω_{rm} is the mechanical rotor speed in rad/s and M is the magnetizing inductance to an average voltage in mH.

TABLE I
PARAMETERS OF THE DTP SEIG

PARAMETER	SYMBOL	VALUE	UNIT
Stator resistance	R_s	0.62	Ω
Rotor resistance	R_r	0.63	Ω
Stator leakage inductance	L_{ls}	6.4	mH
Stator inductance	L_s	206.2	mH
Rotor leakage inductance	L_{lr}	3.5	mH
Rotor inductance	L_r	203.3	mH
Magnetizing inductance (average)	M	199.8	mH
System inertia	J	0.27	kg.m^2
Pairs of poles	P	3	–
Friction coefficient	B	0.012	kg.m^2/s
Nominal frequency	f_a	50	Hz
Electrical power	P_w	15	kW

IV. Simulation Results

MATLAB/Simulink simulation environment has been designed for the DTP SEIG. Simulation tests have been performed to show the behavior of the mathematical model of the DTP SEIG. Numerical integration using the Euler's discretization method algorithm with an integration time of $1\mu s$ has been applied to compute the build up process in the time domain. A block diagram of a DTP SEIG for WECS is provided in Fig. 3.

Fig. 4 shows the inducted voltage from the DTP SEIG with no load. It is considered a capacitor bank of $67\mu F$ and a constant mechanical rotor speed of ω_{rm} = 1000 rpm.

The build up process of the generated voltage is successful, as the amount of reactive power produced from the excitation capacitor is sufficient for the DTP SEIG excitation process to become stable.

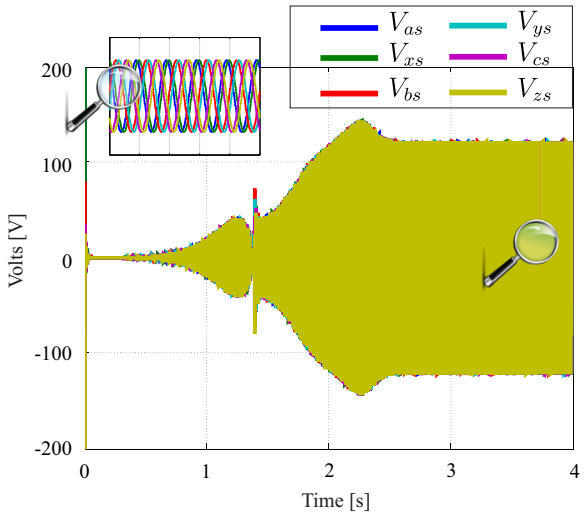

Fig. 4. Output voltage of the DTP SEIG with no load.

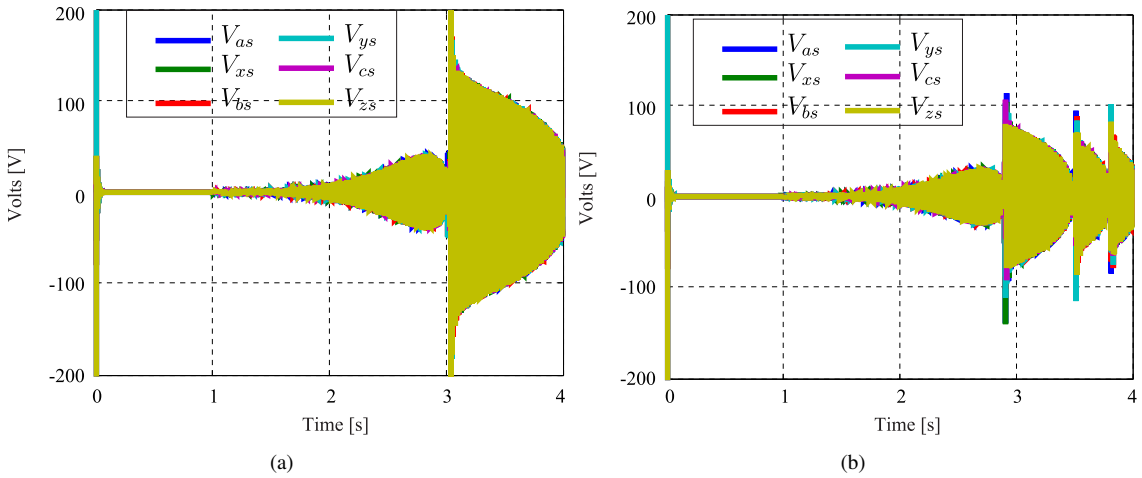

Fig. 5. Output voltage of the DTP SEIG with no load when the self-excitation has failed, (a) $C_{\alpha s} = C_{\beta s} = 40\mu F$; (b) $\omega_r = 772.5$ rpm.

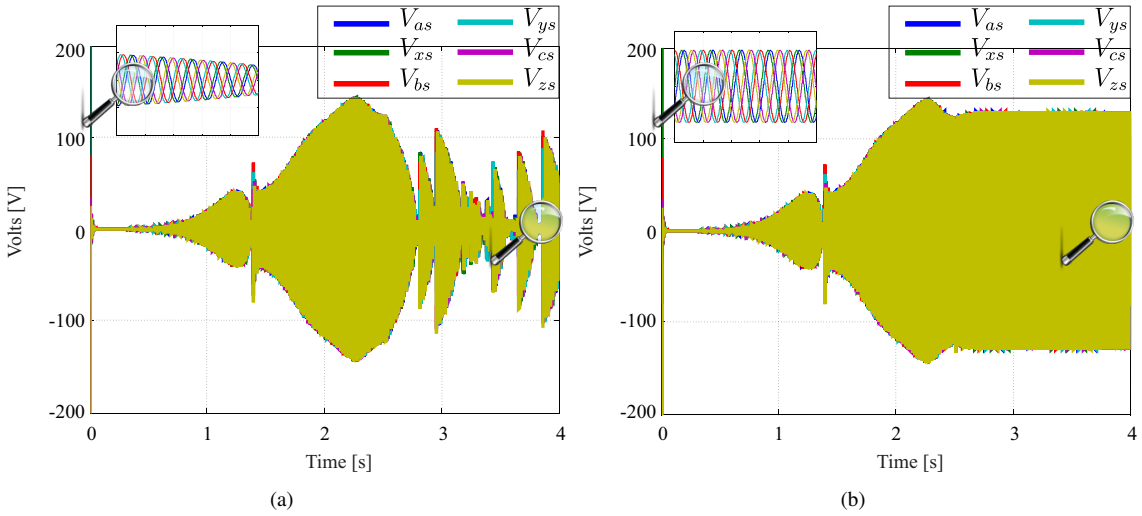

Fig. 6. Output voltage of the DTP SEIG with load, (a) $R_L = 10\ \Omega$; (b) $R_L = 50\ \Omega$.

It is demonstrated in Fig. 5(a) the negative effect of using a capacitor bank of capacitance lower than the minimal calculated on (18), the amount of the reactive power produced from the excitation capacitor bank is insufficient to the excitation process. For this case, it was used a constant mechanical rotor speed of 1000 rpm with no load. It can be obtained a successful excitation process by increasing the mechanical rotor speed to compensate the decreasing of the capacitance. Fig. 5(b) shows the output of the DTP SEIG by using a lower mechanical rotor speed, obtaining an unsuccessful build up process. This is because the mean value of the mechanical rotor speed is insufficient to excite the DTP SEIG, as the output voltage will not stabilize, for this test, it was used a excitation capacitance of $67\mu F$ with no load. Just as the last test, it could be obtained a successful excitation process, this time, by increasing the capacitance in order to compensate the reduced mechanical rotor speed. In Fig. 6(a) it can be observed that the R load, connected at $t = 2.5$ s, did not allowed the self-excitation process to become successful. This is caused by the current generated through the load, the amount needed for the DTP SEIG is more than it can produce. However, in Fig. 6(b), the R load connected to the dual-three phase SEIG requires lower current, so the self-excitation process is successful. Fig. 7(a) shows a build up process of the generated voltage through a RL load, connected at $t = 2.5$ s, particularly for $R_L = 6.7\ \Omega$ and $L_L = 654.4$ mH. It can be seen that the self-excitation process is successful. As for Fig. 7(b), the test consisted in reducing the mechanical rotor speed to 90 % of its nominal value at $t = 3$ seconds, and it can be concluded that the self-excitation process for this particular RL load is insufficient. Then ω_r is augmented to its nominal value 100π rad/s at $t = 5.5$ s, and the self-excitation process is stabilized.

Through a power converter it is possible to connect to DC loads, or through a voltage source inverter for AC multiphase loads of different number of phases, such as five-phase motors, as shown in [14]–[16] or through a matrix converter to different AC loads in [17].

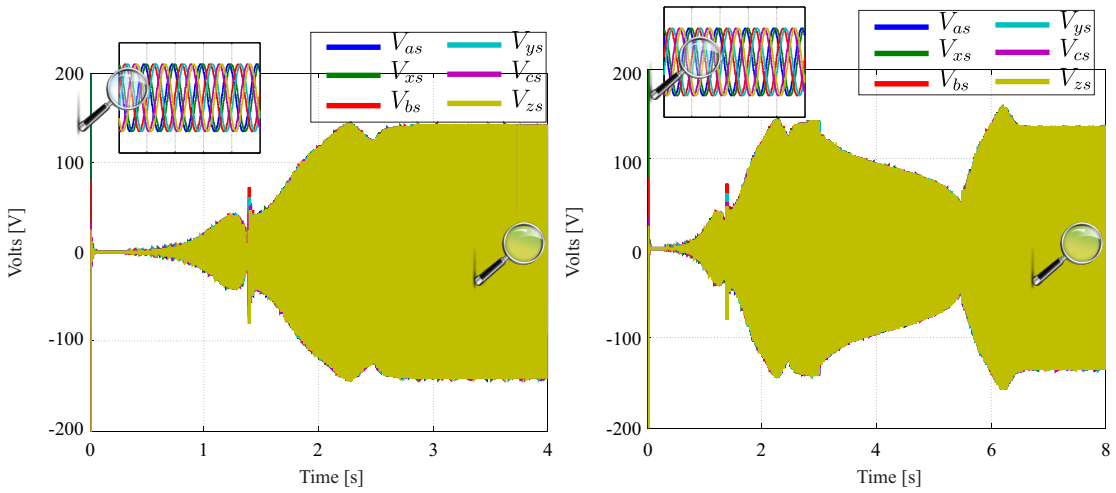

Fig. 7. Output voltage of the DTP SEIG with RL load, (a) ω_r constant; (b) ω_r variable.

V. Conclusion

In this paper, the model of the DTP SEIG in the (α-β)-(x-y) sub-spaces is presented. Since the output voltage and frequency depend on several variables such as: the mechanical rotor speed, the excitation capacitor and the connected load, it is important to perform the steady-state analysis in order to observe its behavior under different conditions. The results have shown that the capacitance of the excitation capacitor must be precisely calculated in order to obtain a successful build up process of the DTP SEIG. The output voltage magnitude depends of the variation of the mechanical rotor speed, where decreasing the rotor speed will lead to decrease the output voltage. This demonstrates the voltage regulation problem of the DTP SEIG when it is used for wind application (rotor speed varying with wind speed varying). The output build up voltage process also follows the variation of the magnetizing inductance. The relationship between the magnetizing inductance and the magnetizing current needs to be obtained experimentally to obtain a very precise model of the DTP SEIG. At last, the load current is another factor which could affect the self-excitation process, so it is important to know the load limits the DTP SEIG can operate to guarantee a successful self-excitation process.

Acknowledgment

Financial support came from CONACYT (Paraguayan Government) 14-INV-101 and PVCT 16-90, and FONDECYT (Chilean Government) into Research Regular 1160690.

References

[1] C. Kalaivani and K. Rajambal, "Modeling and analysis of multiphase induction generator," in *Proc. ICCPCT*. IEEE, 2016, pp. 1–6.

[2] F. Barrero and M. J. Duran, "Recent advances in the design, modeling, and control of multiphase machines: Part I," *IEEE Trans. Ind. Electron.*, vol. 63, no. 1, pp. 449–458, 2016.

[3] E. Levi, "Advances in converter control and innovative exploitation of additional degrees of freedom for multiphase machines," *IEEE Trans. Ind. Electron.*, vol. 63, no. 1, pp. 433–448, 2016.

[4] M. J. Duran and F. Barrero, "Recent advances in the design, modeling, and control of multiphase machines part: II," *IEEE Trans. Ind. Electron.*, vol. 63, no. 1, pp. 459–468, 2016.

[5] T. M. Masaud and P. Sen, "Modeling and analysis of self-excited induction generator for wind energy conversion," in *Proc. ISGT*. IEEE, 2015, pp. 1–5.

[6] J. Rodas, R. Gregor, Y. Takase, D. Gregor, and D. Franco, "Multi-modular matrix converter topology applied to the six-phase wind energy generator," in *Proc. UPEC*. IEEE, 2015, pp. 1–6.

[7] L. Kalamen, P. Rafajdus, P. Sekerak, and V. Hrabovcova, "A novel method of magnetizing inductance investigation of self-excited induction generators," *IEEE Trans. on Magnetics*, vol. 48, no. 4, pp. 1657–1660, 2012.

[8] R. Gunawan, F. Yusivar, and B. Yan, "The magnetizing characteristic in the air gap of the SEIG using Runge Kutta method and correction factor," *Theoretical & Applied Information Tech.*, vol. 72, no. 3, 2015.

[9] J. Dalei and K. B. Mohanty, "A novel method to determine minimum capacitance of the self-excited induction generator," in *Proc. TechSym*. IEEE, 2014, pp. 408–413.

[10] R. Gregor, G. Valenzano, J. Rodas, J. Rodríguez-Piñeiro, and D. Gregor, "Design and implementation of an FPGA-based real-time simulator for a dual three-phase induction motor drive," *Journal of Power Electron.*, vol. 16, no. 2, pp. 553–563, 2016.

[11] M. Ayala, O. Gonzalez, J. Rodas, R. Gregor, and M. Rivera, "Predictive control at fixed switching frequency for a dual three-phase induction machine with Kalman filter-based rotor estimator," in *Proc. ICA/ACCA*, 2016.

[12] Y. Zhao and T. A. Lipo, "Space vector PWM control of dual three-phase induction machine using vector space decomposition," *IEEE Trans. Ind. Applications*, vol. 31, no. 5, pp. 1100–1109, 1995.

[13] H. S. Che and W. P. Hew, "Dual three-phase operation of single neutral symmetrical six-phase machine for improved performance," in *Proc. IECON*, 2015, pp. 001 176–001 181.

[14] O. Gonzalez, J. Rodas, M. Ayala, R. Gregor, M. Rivera, M. Duran, and I. Gonzalez-Prieto, "Predictive current control with Kalman filter observer for a five-phase induction machine operating at fixed switching frequency," in *Proc. ICIEA*, Siem Reap, Cambodia, 2017.

[15] J. Rodas, H. Guzmán, R. Gregor, and F. Barrero, "Model predictive current controller using Kalman filter for fault-tolerant five-phase wind energy conversion systems," in *Proc. PEDG*. IEEE, 2016, pp. 1–6.

[16] J. Rodas, F. Barrero, M. R. Arahal, C. Martin, and R. Gregor, "On-line estimation of rotor variables in predictive current controllers: A case study using five-phase induction machines," *IEEE Trans. Ind. Electron.*, vol. 63, no. 9, pp. 5348–5356, 2016.

[17] S. Toledo, M. Rivera, R. Gregor, J. Rodas, and L. Comparatore, "Predictive current control with reactive power minimization in six-phase wind energy generator using multi-modular direct matrix converter," in *Proc. ANDESCON*. IEEE, 2016, pp. 1–4.